ISIJ International, Vol. 66 (2026), No. 5, pp. 661–672
https://doi.org/10.2355/isijinternational.ISIJINT-2025-205

Virtual Macroetch for Quality Assessment in Complex Continuous Cast Steel Shapes

Gianluca BAZZARO[1)]* and Francesco DE BONA[2)]

1) Danieli & C. Officine Meccaniche SpA, R&D department, Via Nazionale 41, Buttrio, 33042 Italy.
2) DPIA, University of Udine, Via delle Scienze 206, Udine, 33100 Italy.

(*Received July 14, 2025; Accepted February 13, 2026; Advance online published March 2, 2026; Published April 15, 2026*)

In industrial environments, the internal quality of continuously cast steel shapes is typically evaluated afterwards by means of macroetch testing. Nevertheless, this approach becomes increasingly difficult as the product dimensions grow larger. When process parameters change — for example, with an increase in productivity — it is advisable to have a virtual macroetch available to perform a preliminary quality assessment.

In the literature, models exist to predict porosity and microstructure of the final product; however, their validity has been tested only for very simple shapes. In this work, using a travelling-slice approach, a virtual macroetch model was developed for billets and blooms. Comparison with experiments shows that, in the case of billets, the approaches available in the literature provide accurate results. For blooms, however, an accurate prediction of porosity requires a modification of Niyama's criterion, introducing a correction in the exponent q, while Hunt's criterion remain applicable for microstructure.

Based on these results, the case of a beam blank cast at high speed was analyzed. The study confirmed the feasibility of the process, with only a limited increase in porosity and a slight reduction in the equiaxed area in the inner part of the beam blank.

KEY WORDS: steel continuous casting; travelling slice modeling; virtual macroetch; internal quality; beam blank.

1. Introduction

Nowadays, the main challenge for the steel industry is to increase productivity, enabling the coupling between continuous casting and plastic deformation processes—currently feasible only for certain convex cast shapes—through the so-called *hot charging route*. For complex cast shapes such as beam blanks, where concave and convex regions coexist, the calibration of process parameters to achieve the required product quality remains an open issue. The development of models and methods for preliminary quality assessment could significantly contribute to addressing these objectives.

Quality requirements primarily involve two aspects: the distribution of equiaxed and columnar areas across the transverse section, referred to as microstructure, and porosity due to shrinkage, located at the point of final solidification.

Regarding microstructure, it is well established that cast products exhibit a change in grain orientation and size: a thin subsurface chill zone is followed by elongated grains forming a columnar region, from which heat is withdrawn. Near the center, a randomly oriented equiaxed zone appears. The onset of this transition provides a reference for assessing solidification rate: the deeper the equiaxed zone, the faster the solidification. For all shapes, the aim is to maximize the equiaxed fraction of the transverse section. Shrinkage, on the other hand, results from liquid contraction, phase change, and solid thermal contraction. Porosity may arise from shrinkage or gas segregation (*e.g.* hydrogen-induced flakes). In this work, the term porosity will refer exclusively to shrinkage-related defects. While such defects affect all cast shapes, complex geometries such as beam blanks are further subject to additional imperfections (see[1)] for a detailed analysis).

Currently, the only reliable tool for assessing porosity and microstructure is macroetch testing. However, macroetching cannot be performed in real time and is only available after casting. Operational guidelines in continuous casting plants—prescribing parameters such as casting speed, cooling water flow rate, and target surface temperatures—are designed to minimize defects, but cannot guarantee flawless results across all steel grades. When issues arise, corrective measures can only be applied in subsequent casts, and previously produced steel must be managed according to agreed quality standards. A virtual macroetch obtained through simulation would therefore be highly advisable. Moreover, macroetching becomes increasingly difficult as product dimensions increase. Billet macros are common in industrial practice, while bloom macros are less frequent, especially when one dimension exceeds 600 mm. For complex cast shapes such as a beam blank (namely the wider ones) macroetches are rarely available or entirely absent.

Although continuous casting is a well-established technology, computational simulations still face challenges

* Corresponding author: E-mail: g.bazzaro@danieli.it

in reproducing behaviors that cannot be experimentally observed due to to harsh environment (on top of all, high temperatures and scale effects[2]).

With respect to microstructure, there is a seminal paper[3] which predicts the occurrence of columnar to equiaxed transition (CET from here on) analyzing the growth of equiaxed grains ahead of the columnar front during directional solidification. A simple expression was derived to predict the occurrence of fully equiaxed structures, providing a basis for qualitative discussion in more complex casting scenarios. Geometry plays a crucial role in solidification front behavior: in wide rectangles such as slabs, narrow sides can be neglected, whereas in squares, billets, or blooms with small aspect ratios, geometry strongly influences solidification. This effect is even more pronounced in complex shapes with concavities and convexities, such as beam blanks. Furthermore, beam blanks exhibit two solidification endpoints, leading to two potential porosity *loci*, unlike convex shapes where solidification ends at a single central point.

Turning to porosity, Niyama's pioneering work introduced a parameter, later named after him, useful for predicting shrinkage porosity.[4] His experimental approach led to the selection of a parameter, useful for the porosity prediction. Niyama worked on casting of different shapes, from simple (cylinders) to complex ones, spanning on a wide weight interval (from kg to ton). One of the most important outcomes of his research is that the critical threshold below which porosity occurs was proofed to be size independent and, moreover, is not sensitive to steel grade. In[5] a comparison between simulation and experiment is given; object of study is a steel sand mold casting component. The main outcome is that the criterion is shape dependent. In[6] an aluminum die cast component is simulated and experimentally tested; several alloys, with different compositions, were considered and the critical threshold above which porosity appeared was identified. In[7] the Niyama's criterion was applied to a steel ingot weighing tons; although simplifications made, authors claimed a good agreement between simulation and real results. Also in[8] steel ingot was studied, proposing a new criterion which also accounts the effect of pressure gradient in liquid phase; it has been tested and compared with original Niyama's one. Another ingot has been studied with a similar approach in.[9] Carlson and Beckermann made dimensionless the original Niyama's criterion (see[10]): the authors applied their modified criterion to castings in steel, aluminum and magnesium; later on, other authors used it for thin-walled cast components.[11] Results shown that shrinkage porosity may occur with relatively shallow temperature gradients.

So far, no references on steel continuous casting process have been found; first in this field is,[12] where a study on cast slabs was done. The authors adopted the Hunt's model for CET prediction; a wide range of casting speeds, steel compositions, superheat, slab thickness and intensity of secondary cooling have been investigated. Moreover, the effect of electromagnetic stirring (EMS from here on) has been considered; results shown the reliability of Hunt's criterion, although the effect of casting speed and superheat had been recognized as weak on the columnar to equiaxed transition. Later, a paper[13] focused on continuously cast round blooms has published; as in previous article, authors put their attention on how casting speed, primary and secondary cooling intensity affect the CET position. Several diameters, from 210 mm to 410 mm, have been analyzed and observed; some temperature measurements have been performed and compared with model that gave the heat transfer history along caster, together with Hunt's criterion, highlighting the importance of process parameters that influenced the thermal field. Main outcome was the CET dependency on casting speed, superheat and secondary cooling. On the contrary of,[12] superheat seems to play a role; similar conclusions have been drawn in[14] for high carbon continuous cast billets. In[15] the prediction of both CET and porosity in continuously cast billet was proposed for the first time; the authors made a comprehensive job, going in deep on the effect of process parameters considering, among others, also M-EMS and F-EMS. One of the most important contributions has been the modification of both Hunt's and Niyama's criteria; for this latter one a three-stage approach has been given, identifying two different thresholds and not only one as in the original criterion. Talking about Hunt's criterion, two new thresholds have been tested and compared with experiments. An interesting dissertation on the effect of EMS devices is proposed, trying to correlate their action with electrical parameters (such as current and frequency). Two main results came from this paper: a new formulation of Niyama's criterion and the statement in which the authors told their findings are limited to the investigated casting conditions. Successively, some authors[16] suggested a theoretical framework on porosity formation on cast slabs; the implementation of countermeasures to lessen this phenomenon was suggested. Quite recently, the case of semicontinuous cast slabs has been published;[17] as in,[15] authors used both original Hunt's and Niyama's criteria to assess the CET and porosity issues. They performed numerical simulations with and without M-EMS (namely the EMS device in mould) and compared the results with the casted products; an agreement between observations and calculations was found. Moreover, they pointed out the beneficial effect of M-EMS in extending the equiaxed area; it shall be noted that similar conclusions were made by,[15] although on a different cast shape, so demonstrating the usefulness of EMS devices in continuous casting. Recently, same authors have further enlarged the topic in 2023 by means of article,[18] always targeting the slab field.

It is possible to conclude that papers dealing with the application of both Hunt's and Niyama's criteria in continuous casting of steel can be found for semicontinuous casting[17] and continuous casting[12,16] of slabs, as well as for billets[15] and round blooms:[13] no other shapes, even more complex, have been investigated, thus indicating a lack of knowledge for other cast products of industrial interest such as rectangular blooms and beam blanks.

The most representative complex shape in continuous casting is the beam blank, which represents one the cornerstone of the so called "near net shape" cast product. This feeds the subsequent beam rolling process. On the contrary of convex shapes, such as billet, blooms, rounds and slabs, where the last solidified point is the center of the section, beam blank is characterized by a phenomenon that only convex/concave shapes shown: the complete solidification take place at two different times, that means it ends in two different places. This could lead to porosities in different zones, not only in the central point. Beam blanks shown a big variety of dimensions and metric weights, ranging from 280×200×80 mm (width, height and web thickness) up to 1 300×500×140 mm, with masses per unit length ranging from 300 to 2 700 kg/m. A classification can be done based on mass: small beam blanks up to 350 kg/m, medium up to 1 000 kg/m and big ones beyond this threshold. Small ones are cast by monolithic molds, while medium and big need plate molds. To date, the common throughput is around 35 to 40 ton/h for small sections, 50 to 55 ton/h for medium sections and up to 95 to 100 ton/h for big ones. After casting small (also called "light") beam blanks are processed by continuous rolling mills while medium and large (or "heavy") by reversing mills, but in all cases the throughput of single strand does not meet the mill productivity: for this reason, the continuous casters are multistrand and an intermediate furnace placed in between caster and mill, acting as hot buffer, is needed. Nowadays, these plants follow the so called "cold charge" production: products coming from continuous caster loses heat and are put in the furnace at room temperature. This means that a considerable amount of energy shall be given again to the beam blank to reach a temperature (not less than 1 200°C) suitable for

the subsequent plastic deformation process. Since the furnaces are gas fired, a higher product temperature at furnace inlet reduces the enthalpy to be given, resulting in less fuel consumption, lowering carbon dioxide emissions and operational expenditure. The only way to do this is switch to the "hot charge" production route, where beam blanks are put in the furnace at higher temperatures: this means that they must be cast at higher speeds to lessen the heat losses. Another goal of this article is to verify if it is possible to increase more than twice the present casting speed for a medium sized beam blank, still fulfilling the quality requirement of the final product in term of microstructure and porosity.

Thus, the aim of this work is filling the existing gap, developing a tool which makes possible to obtain beforehand a virtual macroetch, targeting the assessment of both CET position and porosity in the case of continuous casting product characterized by more complex shape (such as beam blank); for this purpose the well-known Hunt's and Niyama's parameters (in the original and modified form) will be applied and verified experimentally, demonstrating that further modification of Niyama's criterion is advisable. Finally, it will be shown as virtual macroetch can constitute a suitable tool to improve the continuous casting process. The feasibility of a high casting speed beam blank will be presented, where the complex shape is cast at a double speed, to reach a productivity (actually 50 to 55 ton/h for sizes up to a metric weight of 1 000 kg/m) aiming to make possible the hot charging of cast product to the subsequent rolling process (the target is 120 to 130 ton/h).

2. Theoretical Background

Continuous casting process is first a thermal driven process. To compute the temperature evolution, a convenient and widely used approach is the so called "travelling slice" modeling. A 2D transient thermal model in a Lagrangian framework, in which transversal section of cast product is moving at constant speed from meniscus, where the travelling slice is filled with poured molten steel and solidification starts, till the end of the casting machine: during the motion boundary conditions vary, from heat flux in mould to convection and radiation in the secondary cooling zone.

Since both Niyama's and Hunt's parameters are based on variables that are thermal field depending, they can be well fitted inside a thermal model.

The governing equations are the following:

$$\rho \frac{\partial H}{\partial t} = \nabla \cdot (\lambda \nabla T) \quad \text{..... (1)}$$

$$H = c_p T + L(1 - f_s) \quad \text{..... (2)}$$

where t is time, λ is thermal conductivity, H is enthalpy, T is temperature, ρ is density, c_p is specific heat at constant pressure, L is latent heat and fs is solid fraction.

In any point of the domain is possible to determine a spatial thermal gradient:

$$G' = \frac{\partial T}{\partial n} \quad \text{..... (3)}$$

(where n is the generic coordinate), as well as a time thermal gradient (also called cooling rate):

$$R = \frac{\partial T}{\partial t} \quad \text{..... (4)}$$

Solid fraction can be calculated from temperature:

$$f_S = \begin{cases} 0, & T > T_L \\ 1 - \dfrac{T - T_S}{T_L - T_S}, & T_S \le T \le T_L \\ 1, & T < T_S \end{cases} \quad \text{..... (5)}$$

where T_L and T_S are liquidus and solidus temperatures respectively.

Moreover, speed of solidification in the mushy zone ($0 \le f_S \le 1$) is given by:

$$V = \frac{R}{G'} = \frac{\partial T}{\partial t} \cdot \frac{\partial n}{\partial T} = \frac{\partial n}{\partial t} \quad \text{..... (6)}$$

The assumptions made are: instantaneous pouring of steel at meniscus (whole numerical domain is at T_L plus a superheat from 20°C to 50°C depending to casting conditions), convection in liquid steel negligible, phase transformation proceeds from liquid to solid, latent heat of solidification uniformly released between liquidus and solidus temperatures. Steel properties will be duly explained later in the article.

Travelling slice lies on a plane, *e.g.* the x-y one (z is the casting axis), so the spatial gradient can be defined as:

$$G = \sqrt{\left(\frac{\partial T}{\partial x}\right)^2 + \left(\frac{\partial T}{\partial y}\right)^2} \quad \text{..... (7)}$$

Now all the parameters are known; Niyama criterion is defined as:

$$Ni = \frac{G}{\sqrt{R}} \quad \text{..... (8)}$$

In refs.[16,17] is stated that the condition in which porosity occurs is when $Ni < 1°C^{½} \cdot min^{½}/cm$ (for steel) and shall be evaluated when $f_S = 0.9$.

Hunt criterion can be written as follows:

$$Hu = \frac{G}{\sqrt{V}} \quad \text{..... (9)}$$

The columnar to equiaxed transition is evaluated at $f_S = 0.3$; equiaxed grains are formed when $Hu < Hu_{lim}$, a limit value not easy to be defined, although for the main part of engineering alloys it ranges from 0.2 to $0.4°C \cdot min^{½}/mm^{¾}$. In[17] a value of $0.5°C \cdot min^{½}/mm^{¾}$ is proposed for a medium carbon steel.

As mentioned before, paper[15] proposes a modification of both above parameters; Niyama's one becomes:

$$Ni_{mod} = \frac{G}{R^{0.895}} \quad \text{..... (10)}$$

Unlike original Niyama's criterion, the modified one is characterized by a double threshold: if $Ni_{mod} < 0.5\ K^{0.105} \cdot s^{0.895}/mm$ porosity is completely formed, while for $0.5\ K^{0.105} \cdot s^{0.895}/mm < Ni_{mod} < 2\ K^{0.105} \cdot s^{0.895}/mm$ partial porosity may be observed.

Given this, it is possible to rewrite Eq. (10) in a more general form:

$$Ni_{mod} = \frac{G}{R^q} \quad \text{..... (11)}$$

where q is an exponent that might assume different values for different cast shapes; for a die casted round products, such as the specimens used by Niyama in his original work (please refer to[4]), q=0.5, while for billets (*i.e.* a square shape continuously cast), according to,[15] q = 0.895. In fact, in the case of continuous casting product the previously mentioned authors stated that a better forecast for porosity can be obtained by increasing the q exponent, in order to take into account also the effect of the secondary dendrite arm spacing (SDAS); this topic has been extensively treated in.[19]

As previously mentioned in,[15] the modified Hunt's parameter is given as:

$$Hu_{mod} = \frac{G^{1.8}}{V} \quad \text{..... (12)}$$

The columnar to equiaxed transition occurs when $Hu_{mod} = 4 \cdot 10^9\ K^{1.8} \cdot s/m^{2.8}$; since there were no indications, it has been assumed this value as general (not for a specific steel grade). As the original criteria, also modified ones shall be evaluated at the same solid fraction (respectively 0.9 and 0.3).

The authors of[15] highlight that proposed thresholds are limited to the casting conditions considered in their work (150 × 150 mm billet cast at 2.2 m/min) and cannot be generalized.

3. Numerical Approach to Achieve a Virtual Macroetch

As stated in the previous paragraph, continuous casting is fundamentally a heat-transfer process, in which heat is removed from molten metal to produce a solid strand with the desired cross-sectional shape and size. Models capable of predicting temperature distribution and the growth of the solidifying steel shell are essential for design, trouble-shooting, and process control. Such models should indicate whether specific operating conditions (*e.g.*, casting speed, secondary cooling) may lead to product defects. Although significant progress has been made in numerical modeling of continuous casting since the pioneering studies of the 1980s, the prediction of defects affecting the cast product remains at an early stage, as written in.[2] The challenge for modelling is to predict something of practical use to operative personnel, such as the formation of some defects. Over the years, advances have been achieved in predicting surface and shape problems, such as rhomboidity in square billets, bulging in blooms and slabs, macrosegregation, and crack formation. Nevertheless, the task remains complex, as continuous casting, like most industrial processes, is governed by a highly interrelated system of physical phenomena.

To provide a rapid tool for generating virtual macroetches, a two-dimensional transient thermal finite element model has been developed, adopting the travelling-slice approach: equations from (3) to (11) were written in a user subroutine which has been executed with the model. Further details will be given in the case study paragraphs.

Temperature dependence of the thermal properties was evaluated by means of the numerical procedure implemented in a computer software called IDS (see[20]), considering the real kinetics of the solidification process, which occurs in non-equilibrium conditions. Because IDS provides different values for thermal conductivity for liquid and solid phases in the mushy zone, the lever rule is used to define thermal conductivity used in calculations:

$$\lambda = \lambda_S \cdot f_S + (1 - f_S) \cdot \lambda_L \quad \ldots\ldots\ldots\ldots\ldots\ldots (13)$$

Three different steel grades were used; their chemical composition is given in **Table 1**, as well as their physical parameters in **Table 2**. It shall be pointed out that first two grades are the real ones from which macroetches have been taken, while last one has a typical composition for beams.

Table 1. Chemical composition.

Element [%]	Steel grade C63	Steel grade 20CrMnTi	Steel grade A615 Gr60
C	0.637	0.204	0.270
Mn	0.999	0.951	0.930
Mo	0.005	0.149	0.100
Ni	0.017	0.302	0.130
Cr	0.101	1.153	0.120
Ti	0.001	0.062	–
V	0.002	0.001	–
Nb	0.003	0.002	–
Si	0.241	0.272	0.240
Cu	0.012	0.006	0.300
Al	0.001	0.001	0.025
P	0.015	0.028	0.005
S	0.007	0.021	0.020
N	0.005	0.004	–
Fe		Balance	

For steel grade 20CrMnTi enthalpy and thermal conductivity are plotted respectively in **Figs. 1** and **2**. The temperature trends among these three steel grades are not so different: for this reason, only one is represented in figure.

In steel industry it is well known that one of the most powerful countermeasures to be taken to improve internal quality is the use of EMS devices: these might improve the internal quality, mainly reducing porosity. These devices stir the molten steels inside mould (M-EMS) or along cast strand (S-EMS and F-EMS) by means of Lorentz forces created by electromagnetic field; they are typically adopted for special steel grades. Other steel grades, namely structural ones, are not subjected to stirring and are much prone to undesired effects previously described. When special steel grades are produced, electromagnetic stirring is typically adopted. Steel grades are considered special when the carbon content is high (typically more than 0.77%, although there is not a precise threshold) or if the sum of alloying elements such as Cr, Mo, Ti, Nb, V and Si reaches at least 1.5%. Among

Table 2. Physical parameters.

Parameter	Steel grade C63	Steel grade 20CrMnTi	Steel grade A615 Gr60
Liquidus temp. [°C]	1 479	1 509	1 507
Solidus temp. [°C]	1 372	1 436	1 435
Latent heat [kJ/kg]	320.39	303.73	307.70

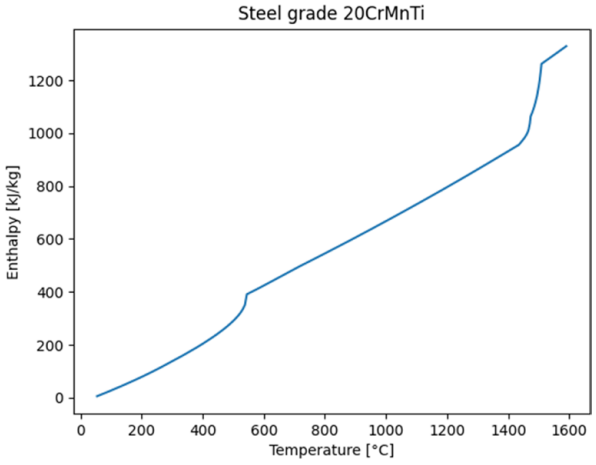

Fig. 1. Enthalpy as function of temperature. (Online version in color.)

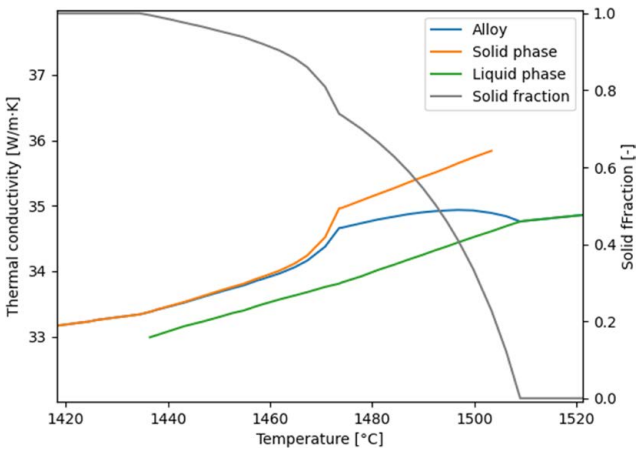

Fig. 2. Contribution of liquid and solid phases to thermal conductivity of steel grade 20CrMnTi. (Online version in color.)

the three steels considered in this work, according to the aforementioned considerations, only 20CrMnTi can be considered a special grade and thus suitable to undergo EMS.

In a continuous casting machine three types of electromagnetic devices can be present: mould stirrers (M-EMS) which deploy their magnetic field inside the mould and operate al low frequencies (up to 5 to 6 Hz), strand stirrers (S-EMS) located in the cooling chamber and final stirrers (F-EMS) placed a little bit before the point in which the casted product is completely solidified; these latter ones adopt higher frequencies (up to 50 Hz). Aim of this paper is not to explain purposes and technology of EMS: an extended and comprehensive recap on this topic is given in[21] and,[22] as well as test on billet surface quality modifying electromagnetic parameters has been reported in[23] and an optimization of mould stirring parameters is given in.[24] An interesting evaluation of EMS effect on solidified structures can be found in,[25] as well as in[26] for big round blooms with all stirrers acting. From computational perspective, the inclusion of electromagnetic effects in a continuous casting model requires a great effort, making mandatory a transient CFD approach (LES better than RANS, as stated in[2]). Many authors tackled this challenging topic, resulting in several papers (*i.e.* see:[27,28]). Such approaches are not suitable to be implemented in a travelling slice model as described in this paper. An alternative way to include the electromagnetic effects is needed. A hint to solve this issue comes from,[17,18] where a simplified procedure is proposed: since EMS devices promote stirring in liquid steel, this results in a higher turbulence at solid/liquid interface (thermal convection is significantly enhanced). This effect is described assuming an increased thermal conductivity of liquid part only. Equation (13) may be amended as follows:

$$\lambda = \lambda_S \cdot f_S + (1 - f_S) \cdot \beta \cdot \lambda_L \quad \text{..... (14)}$$

where β is a coefficient that spans from a value of 2 if there are no electromagnetic devices acting on the product, to a value of 10 when the magnetic field developed by stirrers is maximum. A more precise evaluation of coefficient β can be found in,[15] where it is linked to the electrical parameters (such as current and frequency) of EMS devices for a certain billet size (150 mm). Direct consequence of the above statement is that β shall vary over the whole curvilinear abscissa (*i.e.* the trajectory of the center section starting from meniscus), considering the presence of EMS devices if any (see **Fig. 3** as example containing generic data, not directly related to the arrangement outlined in this paper). The EMS affected zone is assumed to be twice of stirrer length.

4. FE Modeling

To verify if all the statements and assumptions made in previous paragraphs are working properly, a comparison with real cast products is mandatory. For this reason, the illustrative cases of a billet and of a bloom were selected and reproduced with the model to get the virtual macroetch and compare it with real one. It must be pointed out that these two sections are fully representative of continuous cast shapes, since they account about 82% of long product castings.

Models have been built using commercial FE code MSC Marc; their aim is to provide the porosity estimation, as well as microstructure assessment, for a given set of process parameters such as casting speed, primary and secondary cooling intensity and steel grade. Since in steel continuous casting process advection of heat by the moving strand is far higher than conduction in casting direction, a Lagrangian approach with a slice moving down through the strand seems the right choice to achieve a suitable accuracy with a feasible computational effort. A deeper explanation on how travelling slice model is built may be found in.[29] In all models different thermal loads are adopted: in mould a heat flux is applied, while for secondary cooling a heat transfer coefficient (and related bulk temperature) and radiation are used; values are reported in **Tables 3** and **6**. Moreover,

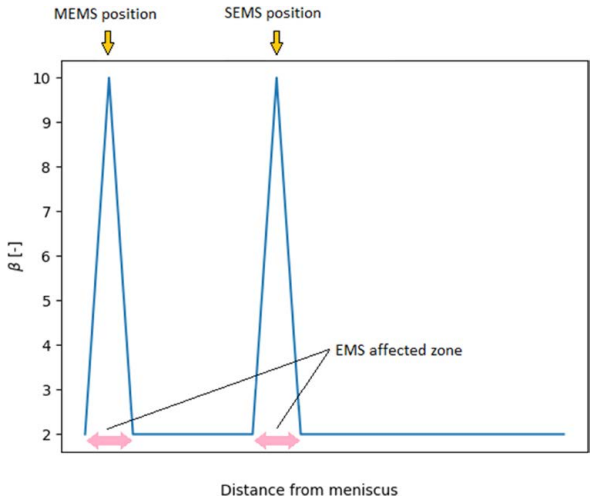

Fig. 3. Trend of beta parameter along casting direction. (Online version in color.)

Table 3. Simulation parameters for billet and bloom.

	Case 1 (Billet)		Case 2 (Bloom)	
Dimensions at mould exit [mm]	161.5 × 162.7		390.0 × 461.0	
Steel grade	C63		20CrMnTi	
Mould EMS, length [mm]	–		590	
M-EMS pos. from meniscus [mm]	–		419	
Casting speed [m/min]	2.46		0.45	
Superheat [°C]	32		35	
Average mould heat flux [kW/m²]	1 938		957	
Mould (length/meniscus) [mm]	1 000 mm	165 mm	780 mm	150 mm
Sector 1 (length/HTC)	450 mm	844 W/m²·K	350 mm	390 W/m²·K
Sector 2 (length/HTC)	1 000 mm	562 W/m²·K	1 200 mm	276 W/m²·K
Sector 3 (length/HTC)	1 000 mm	472 W/m²·K	1 800 mm	252 W/m²·K
Sector 4 (length/HTC)	2 350 mm	295 W/m²·K	–	
Sector 5 (length/HTC)	2 350 mm	247 W/m²·K	–	

the occurrence of phase change during cooling is managed through the uniform release of latent heat between liquidus and solidus temperatures.

In the two cases a fine mesh has been used, to be able to catch the central porosity, aiming to an element size of 1 mm × 1 mm; billet counts 6 887 nodes, while bloom reaches 45 261 nodes. All models adopt four node quadrilateral elements. Double symmetry may be used, resulting in one quarter model (see **Fig. 4**).

First case is a high carbon billet, second one is a bloom of special steel. As shown in Table 3, they have been cast on different continuous casting machines. It must be pointed out that average mould heat flux has been derived from primary water flow rate and temperature difference, for cases 1 and 2, while is hypothesized for case 3.

Heat transfer coefficients have been calculated from cooling water flow rates in each sector according to;[30–32] as did for primary cooling, water flow rates are real for cases 1 and 2 and hypothesized for case 3. For all cases the model is bidimensional thermal transient. From computational perspective, models are not expensive: a single run takes from 280 s (case 1) to 2 290 s (case 3) on a 64-bit 8-processor (Intel Core i7-8850H) PC with 64 GB installed RAM.

5. Virtual and Real Macroetch of a Billet: Results and Discussion

The computed temperature evolution along casting direction for billet continuous casting is visible in **Fig. 5**; no experimental data are available for comparison, anyhow the reliability of travelling slice approach is proven. In **Fig. 6** the distribution of Niyama's parameter on the whole transversal section is given: it is similar to the one given in,[15] although steel grade and casting conditions are different.

Simulation gives an area below threshold of 3.6 mm diameter (original Niyama's criterion), 2.0 mm diameter (modified criterion, first threshold) and 5.1 mm (modified criterion, second threshold); these values must be compared with the real macroetch (see **Fig. 7**) where measured porosity is a circle of 5.0 mm diameter. All these values except modified criterion first threshold, are listed in **Table 4**. It shall be outlined that measurement has been done via image recognition since is not an easy task to correctly identify the shape of porosity.

The obtained results confirm the observation done by,[15] *i.e.* the Niyama's parameter underestimates the porosity dimension. A more accurate forecast is given by the modified approach, as mentioned in Par. 2, because the influence of the SDAS is considered by increasing the value of the q exponent in Eq. (11). It can be thus concluded that modified Niyama's parameter with q=0.895 seems suitable to describe the porosity in a billet.

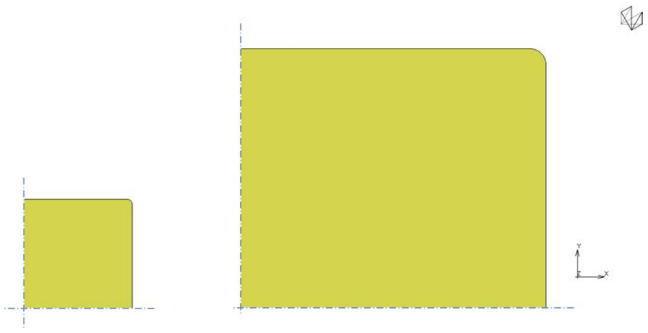

Fig. 4. Models for case 1 (left) and case 2 (right). (Online version in color.)

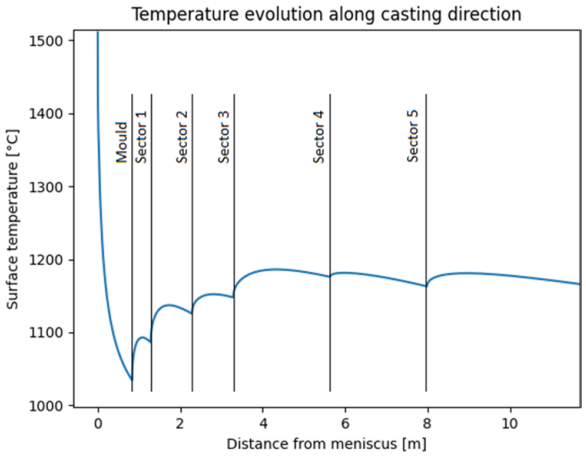

Fig. 5. Billet continuous casting: temperature evolution (detail of the first part of machine). (Online version in color.)

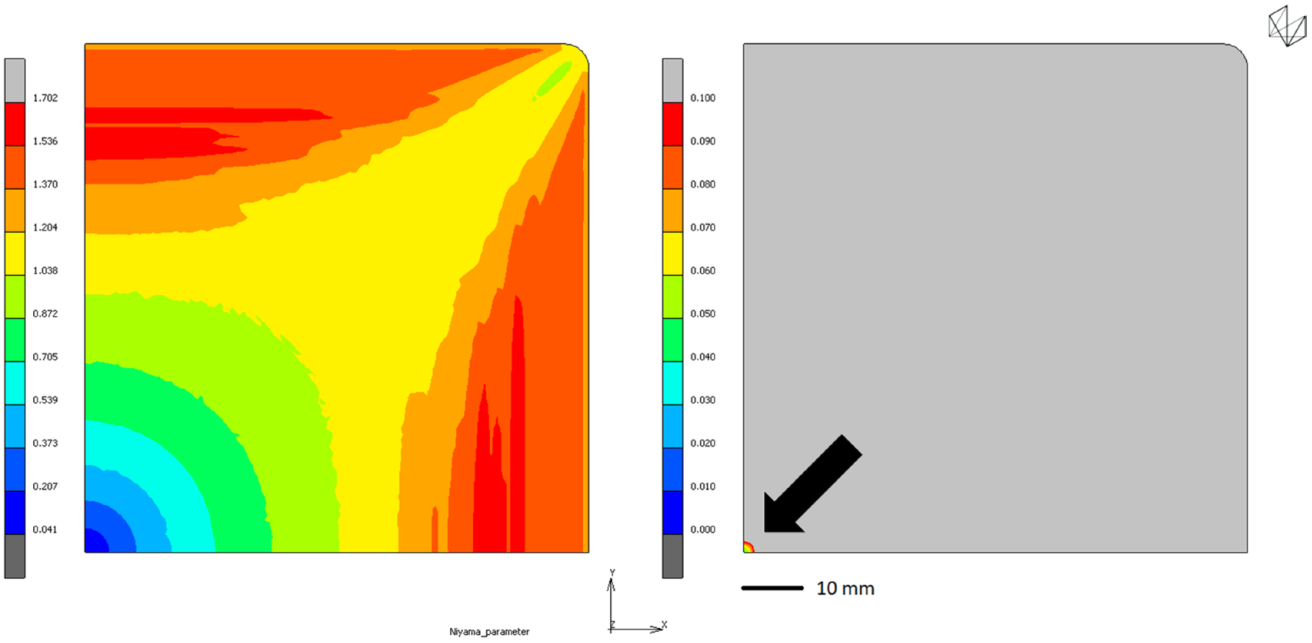

Fig. 6. Billet virtual macroetch: distribution of Niyama parameter (left) and zone where is less than threshold (right, indicated by arrow, original criterion). (Online version in color.)

6. Virtual and Real Macroetch of a Bloom: Results and Discussion

Unlike the billet case, for the bloom one, is possible to make comparison on both Niyama's and Hunt's criteria. It shall be pointed out that another difference with billet case, is the presence of M-EMS (see Table 3). **Figure 8** represents the surface temperature evolution. As in case 1, the image shown in **Fig. 9** gives the distribution of original Niyama's parameter. From simulation has been obtained an oval shape of 5.0 mm (along × axis) by 6.2 mm (along y axis), while image recognition (see **Fig. 10**) gave 2.9 mm (along × axis) by 5.8 mm (along y axis). The modified Niyama's parameter instead led to a porosity area of 1.6 mm by 2.1 mm (first threshold) or 8.4 mm by 10.8 mm (second threshold). As for the billet case, above values except first threshold of modified criterion are given in Table 4. It is visible that original Niyama's criterion gives an overestimation of porous area, while the modified with q = 0.895 (for billets) makes a huge overestimation; to overcome this wrong forecast, a fitting on q exponent has been done. After several attempts made via sim-

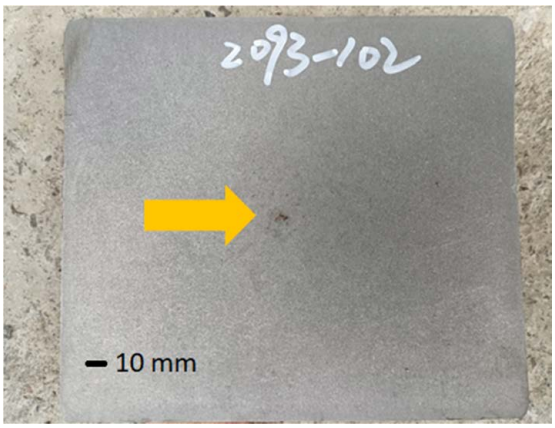

Fig. 7. Billet real macroetch (case 1, porosity highlighted). (Online version in color.)

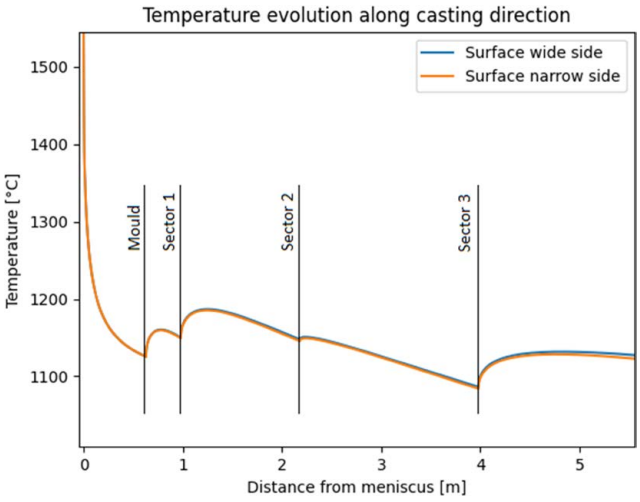

Fig. 8. Temperature evolution for bloom continuous casting (detail of upper part of machine). (Online version in color.)

Table 4. Comparison for porosity (third and fifth columns relative error of estimated porosity affected area).

	Case 1 (Billet)		Case 2 (Bloom)	
Measure (real macroetch)	Ø 5.0 mm		2.9 mm × 5.8 mm	
Original Niyama's criterion	Ø 3.6 mm	− 23%	5.0 mm × 6.2 mm	+ 84%
Modified Niyama's crit. (as per[15])	Ø 5.1 mm	+ 4.8%	10.8 mm × 8.4 mm	+ 433%
Modified Niyama's crit. (present work, q = 1.3)	n. a.		3.0 mm × 5.6 mm	− 0.1%

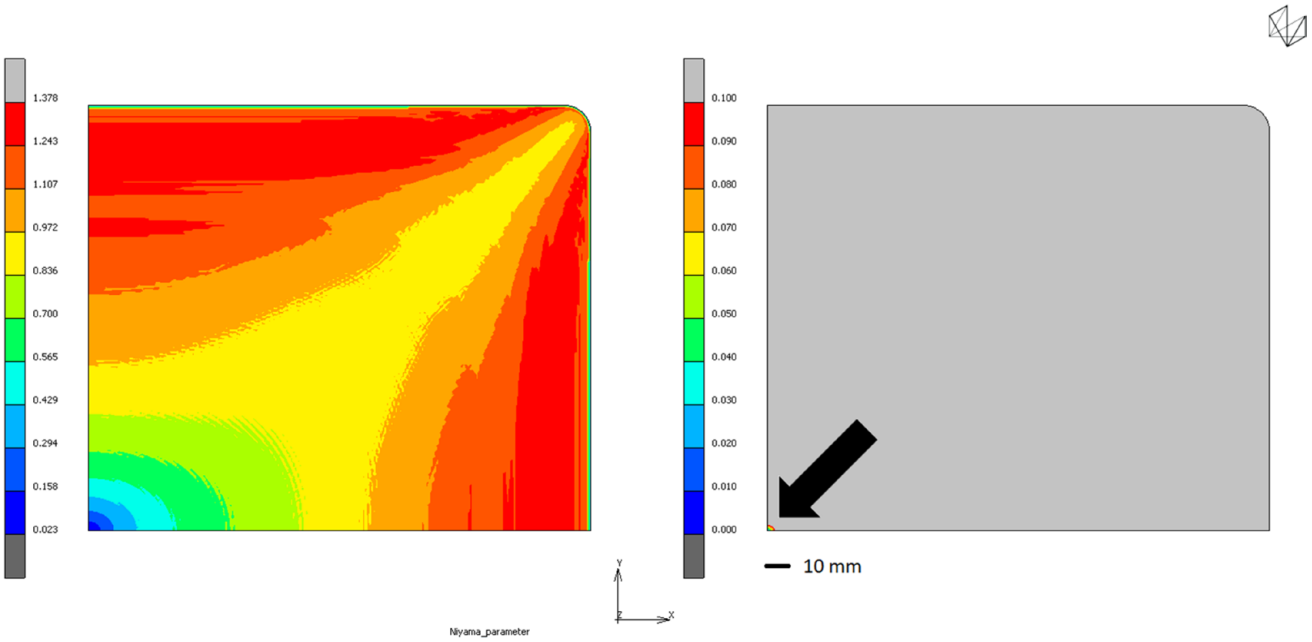

Fig. 9. Bloom virtual macroetch: distribution of original Niyama's parameter (left) and zone where is less than threshold (right). (Online version in color.)

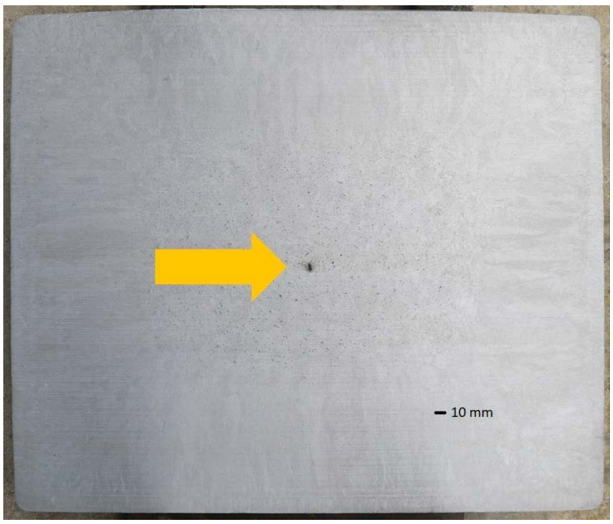

Fig. 10. Bloom real macroetch. (Online version in color.)

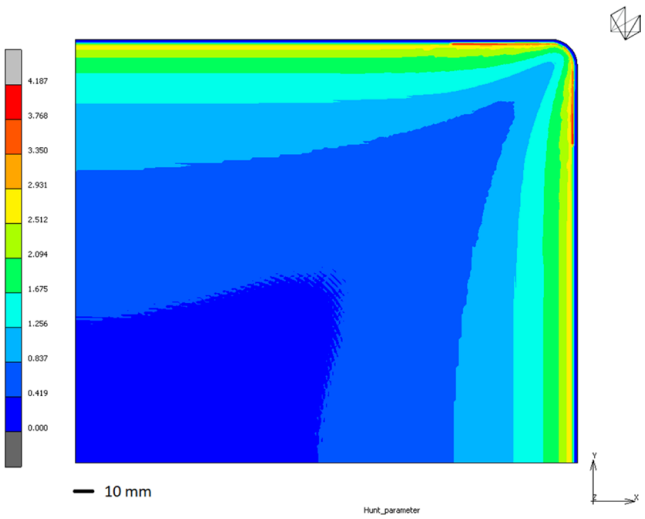

Fig. 11. Bloom: original Hunt's parameter. (Online version in color.)

ulations, it has been found q = 1.3 as best fit value. This result can be justified considering the effect of SDAS mentioned in Paragraph 2. According to,[19] SDAS is not only function of cooling rate, but is affected by time spent in the mushy zone too. Is well know that blooms have a longer solidification time with respect to billets; this leads to a higher permanence in solid-liquid region, thus a bigger SDAS occurs and consequently also a higher value of q. Since q exponent can be considered as the sum of the term 0.5 (original Niyama's criterion) and a correction factor related to SDAS, it follows that blooms must show a higher value of abovementioned correction factor with respect to billets and consequently a higher q value. In conclusion, it can be said that numerically obtained q exponent also finds a theoretical justification.

In Fig. 10 CET can be clearly observed, while **Fig. 11** gives the distribution of original Hunt's parameter.

While Niyama's parameter is claimed to be steel grade independent, Hunt's one is weakly related to the cast steel; to establish the threshold for columnar to equiaxed transition, a test should be conducted. The authors make the choice to assess the right value by means of a bibliographic review. The most authoritative reference is,[17] which fixes the CET onset at $0.5°C \cdot min^{½}/mm^{¾}$; a second reference is given by,[15] reporting a value of $4 \cdot 10^9$ $K^{1.8} \cdot s/m^{2.8}$ (modified Hunt's parameter) for a not alloyed low carbon steel. It shall be underlined that steel grade in[17] has a different carbon content (0.4% instead of 0.204%) but the content of alloying elements, such as Cr, Mo, Mn and Si, shown not a so big difference; for the comparison purposes the same threshold is adopted. In **Fig. 12** the simulation result with contour line 0.5 is superimposed to the macro etching taken from continuous caster. It shall be noted that the real product geometry does not totally fits with numerical domain; this is due to load (*e.g.* effect of liquid steel pressure) not included in the travelling slice model, which is a purely thermal one. As a direct consequence, a small misalignment at the edges, especially the upper one, is detected although this does not affect the area where CET occurs.

Figure 13 is a graphical representation of original Hunt's parameter along x and y axes, from which can be conveniently located transition onset, respectively 130.0 mm and 86.6 mm; modified Hunt's parameter gives 132.7 mm and 90.4 mm. As for porosity, the identification of transition line is not indubitable and is observer related. The image recognition gives 131.9 mm (in width direction) and 92.0 mm (in thickness direction). **Table 5** recaps the obtained results and compare them with the experimental ones. As visible, both original and modified Hunt's criterion furnish similar results; modified one is closer to real macroetch.

It is thus possible to conclude that in the case of a bloom,

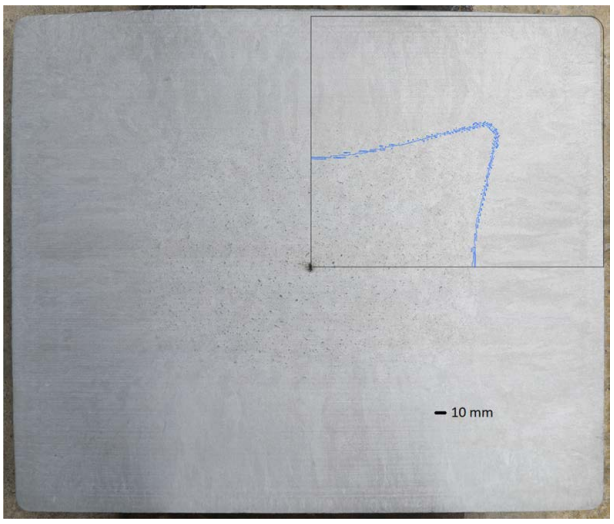

Fig. 12. Overlap of simulation result on the bloom's macroetch. (Online version in color.)

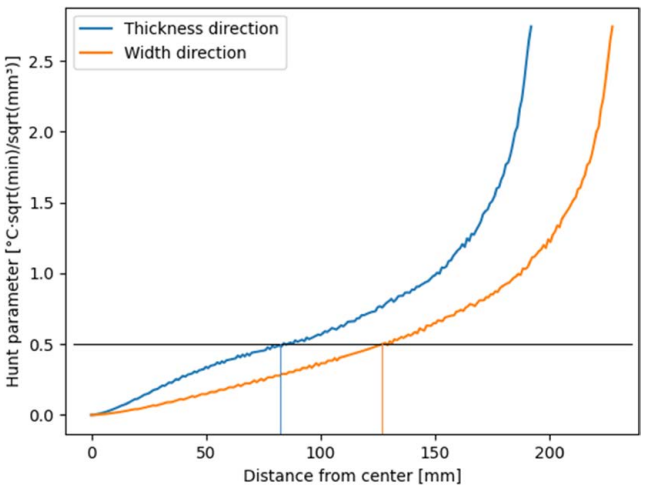

Fig. 13. Trend of original Hunt's parameter on width (orange) and thickness directions (blue). (Online version in color.)

porosity can be still well forecasted by using the modified Niyama's parameter, where q=1.3 (see Eq. (11)). The columnar to equiaxed transition (CET) seems slightly better described by the modified Hunt's parameter.

7. Proof of Concept of a High-speed Beam Blank Casting Process

In this case, a travelling slice approach was also adopted, and a fine mesh was used, in order to be able to catch the central porosity, aiming to an element length of 1 mm × 1 mm (44 971 nodes in this case). Due to the different boundary conditions respectively at inner radius, outer radius and lateral sides (summarized in Table 6), in this case only one symmetry condition can be used (see **Fig. 14**). With respect to the case of billet and bloom, in this case the average mould heat flux and the heat transfer coefficients cannot be derived from primary water flow rate and temperature difference measured in the real plant but can be only hypothesized. **Figure 15** reports the surface temperature evolution. At mould exit a reheating in first sector followed by a smooth cooling in the subsequent ones has been calculated. These trends are in line with expectations and similar to,[33] although sizes and casting speed are different. The different cooling path, especially between inner radius and outer radius, leads to a not symmetric solidification locus in y direction: in other words, the last solidified areas are located a little bit above x axis.

Table 5. Comparison for CET, bloom only (third and fifth columns relative error of the estimation).

	Thickness direction		Width direction	
Measure (real macroetch)	92.0 mm		131.9 mm	
Original Hunt's criterion	86.6 mm	− 5.9%	130.0 mm	− 1.4%
Modified Hunt's criterion	90.4 mm	− 1.7%	132.7 mm	+ 0.6%

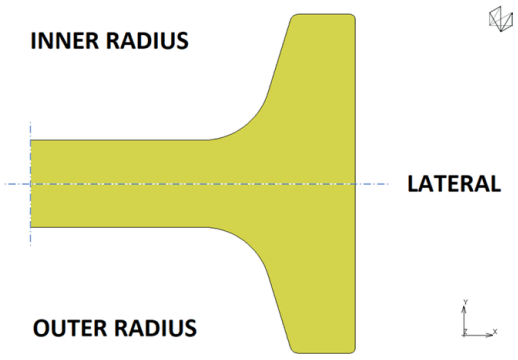

Fig. 14. Beam blank model. (Online version in color.)

Figure 16 represents the solid fraction at center and in the so called "triple point": is clearly visible that solidification is completed at different distances from meniscus, for triple point 15 m after the center. It shall be noted that the higher is the casting speed, the higher this difference will be: generally speaking, this is not a drawback, anyhow it highlights

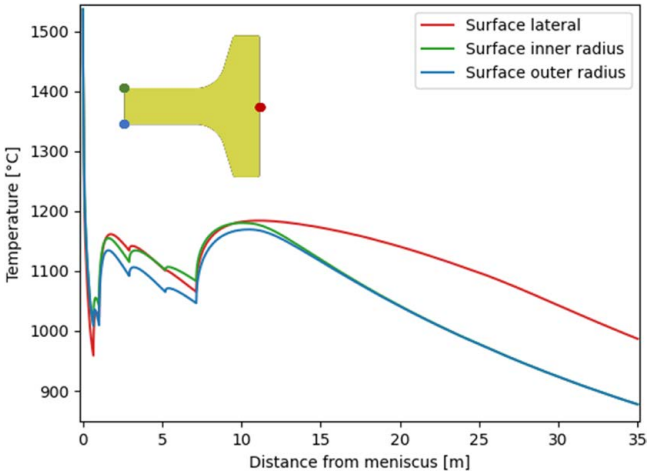

Fig. 15. Case 3: temperature evolution along casting direction. (Online version in color.)

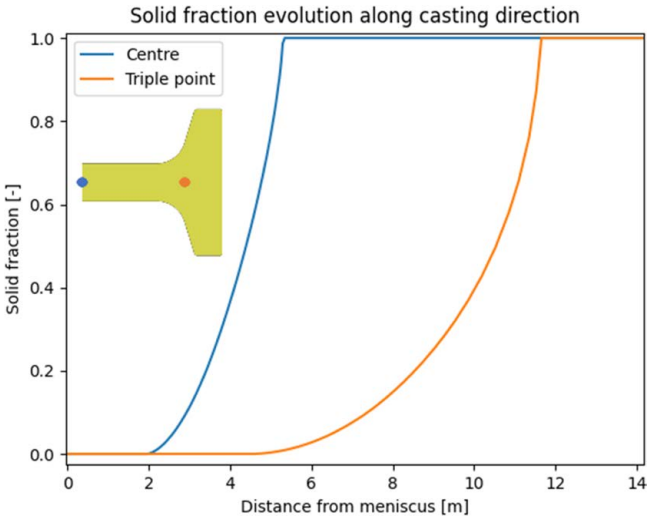

Fig. 16. Solid fraction trend along casting direction in two different locations. (Online version in color.)

Table 6. Simulation parameters for beam blank.

	Case 3 (Beam blank)			
Dimension at mould exit [mm]	690 × 360 × 93 (web thickness)			
Steel grade	A615 Gr60			
Casting speed [m/min]	2.2			
Superheat [°C]	30			
Avg. mould heat flux in/out [kW/m^2]	1 911			
Avg. mould heat flux lateral [kW/m^2]	2 034			
Mould (length/meniscus)	780 mm		120 mm	
Sector 1 (length/HTC in, out, lateral)	0.36 m	1 117 W/m^2·K	1 251 W/m^2·K	1 117 W/m^2·K
Sector 2 (length/HTC in, out, lateral)	1.90 m	540 W/m^2·K	578 W/m^2·K	493 W/m^2·K
Sector 3 (length/HTC in, out, lateral)	2.28 m	423 W/m^2·K	472 W/m^2·K	428 W/m^2·K
Sector 4 (length/HTC in, out, lateral)	1.95 m	382 W/m^2·K	421 W/m^2·K	412 W/m^2·K

the need to extend the containment and supporting zone till the complete solidification will be totally achieved.

Figure 17 shows solid fraction and temperature distributions in the transversal section in two different instants of casting process: close to solidification end at center point (top images) and close to solidification end at triple point (bottom images). Especially in top images, is visible that the still liquid portion is quite extended over the whole transversal section; this behavior is due to the complex shape and has not been observed in other cast shapes such billets and blooms.

Having two solidification end points may led to doubling the unavoidable phenomena related to it; it is well-known that segregation at the end point of solidification determines the unwanted separation of steel alloying elements, which occurs during the transition from the liquid to the solid state. As elements have different melting temperatures and different solubility in the solid state, those with higher melting temperatures tend to solidify first, while elements that have lower solubility concentrate in the remaining areas, leading to uneven distribution which can affect the mechanical properties of the final material.

Coming to the internal quality assessment, some considerations have to be done before. As stated in the introduction, macroetching testing procedure becomes more difficult or even impossible, when dimensions tend to be big. Another reason that makes the beam blank macros unusual is that the casting speed is generally quite low: this lead to avoid major issues (although is not guarantee of "defect free" product). Given these statements, it shall be pointed out that the outcomes of the simulation done with boundary conditions listed in Table 6 (*e.g.* the high casting speed case) will be compared with another simulation at lower speed, taken as reference both for porosity as well as CET. To avoid making this paper longer, extensive results for the standard speed case (0.9 m/min, same dimension reported in Table 6), as well as boundary conditions, are not given.

It shall be noted that beam blank is more similar to a bloom rather than a billet; given the tuning of parameters explained in previous paragraph, the modified Hunt's and Niyama's criteria (both versions) will be used. The distribution of modified Niyama's parameter (the version introduced in this paper) is shown in **Fig. 18**: in right part contours are limited to the $0.1°C^{½}·min^{½}/mm$ threshold in order to put in evidence the porous affected area (colored). As expected, the simulation predicts two areas where porosity develops: a wide but thin one in central part of product (A) and a spot in the triple point (B), although the amount of surface below threshold is little compared to the transversal section. Is interesting to note the different extensions of areas coming from the three versions of the criterion, as visible in **Table 7**. For the central part the biggest area is given by original criterion, while the two modified are quite close; for triple point original gives far higher area than modified. According to the authors, the modification proposed in this work should be the more realistic since it has been tuned on a bloom.

The comparison with standard casting speed case, leads to results listed in **Table 8**; taking as reference the criterion modified by this work, is clearly visible the effect of increased casting speed with a higher extension of porosity in the central part (+ 60%), while for triple point it might be said there are no significant changes. Nevertheless, it must be underlined that affected porosity area, in absolute values, is far below the transversal section of cast shape.

Regarding the equiaxed and columnar distribution on the whole section, **Fig. 19** gives the modified Hunt's parameter distribution for high casting speed case; it shall be emphasized that contours values differ from ones in Figs. 11 and 13 because these latter two are referred to original Hunt's parameter. Results shown an outer layer of columnar structures 41 to 63 mm thick, depending on the position. Approximately the 12.2% of cast product area belongs to equiaxed morphology (with no stirring devices at all); for standard casting speed case this value is 15.5%. For comparison, in the bloom represented in Fig. 10 the equiaxed

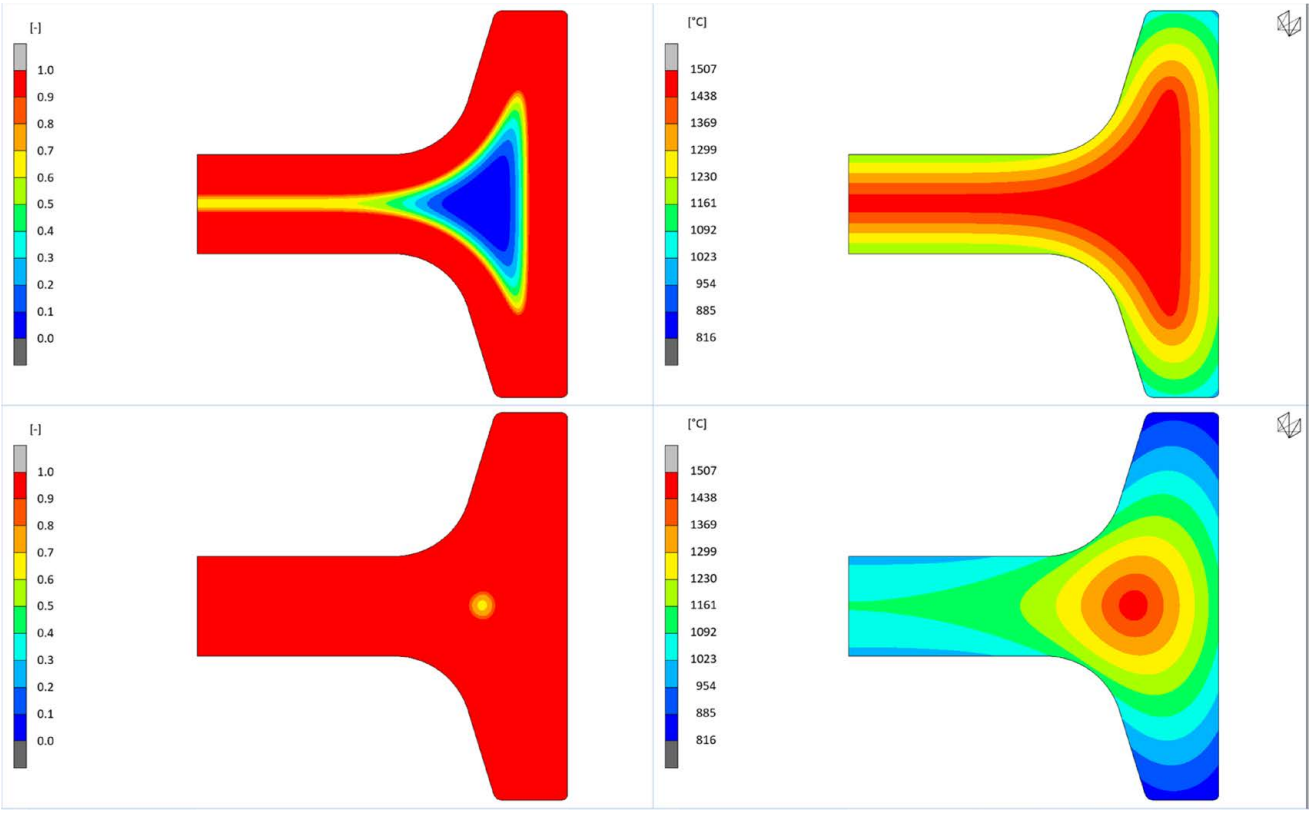

Fig. 17. Top: solid fraction just before solidification end at centre (left) and temperature distribution at same time (right). Bottom: solid fraction just before solidification end at triple point (left) and related temperature distribution (right). (Online version in color.)

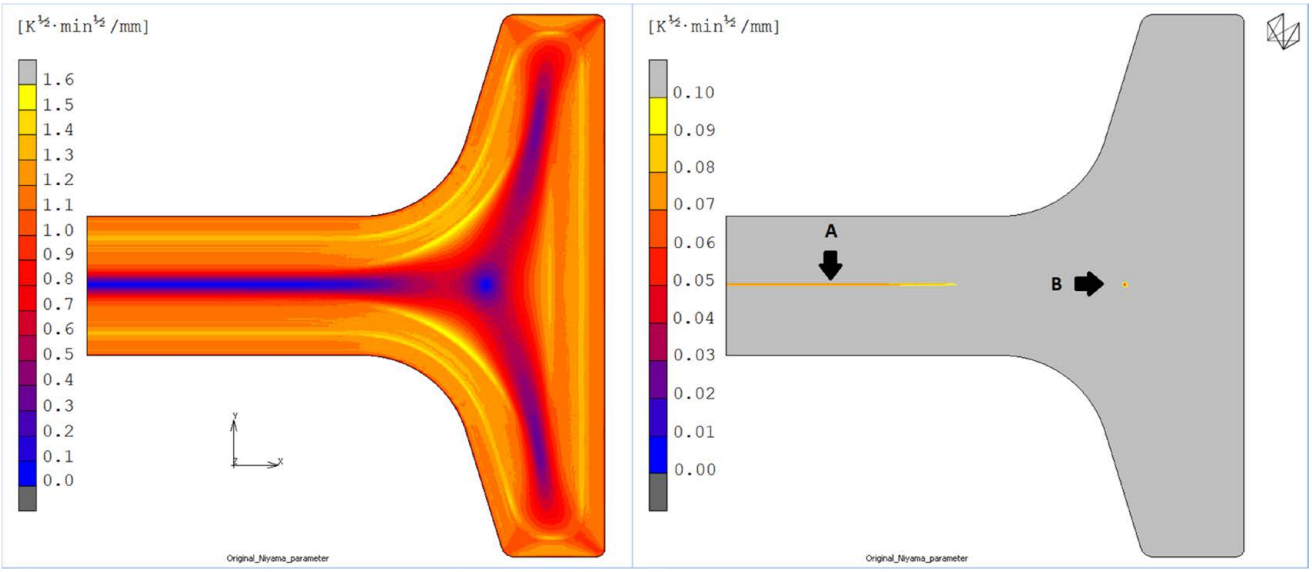

Fig. 18. Distribution of modified Niyama's parameter (left) and predicted areas of porosity (right). In right image contours are limited to porosity threshold to highlight the porous areas. (Online version in color.)

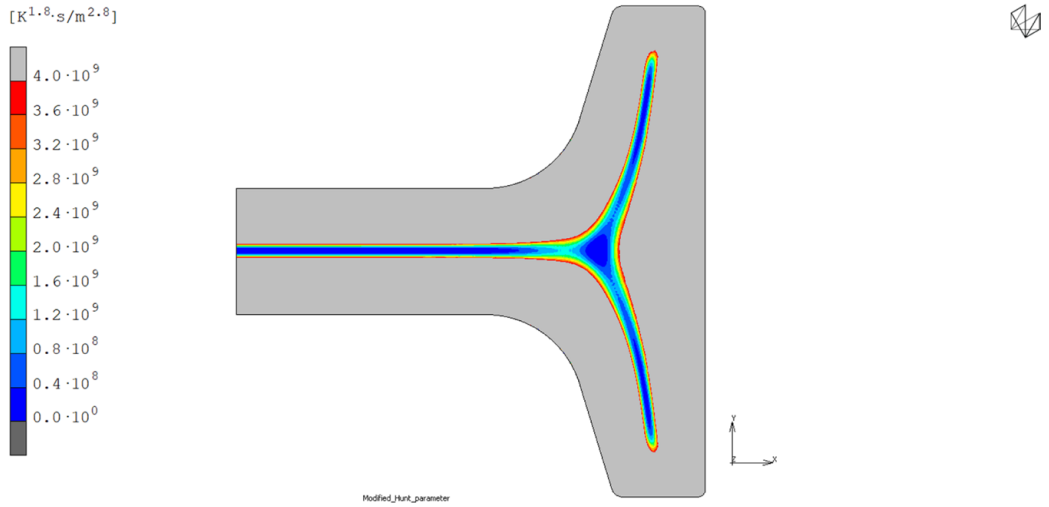

Fig. 19. Modified Hunt's parameter (colored part where equiaxed morphology is formed). (Online version in color.)

Table 7. Niyama's criteria outcomes: extension of areas where porosity might occur.

	Central part (A)	Triple point (B)
Original criterion	210.1 × 8.4 = 1 765 mm^2	23.4 × 29.3 = 538 mm^2
Modified criterion (as per[15])	174.5 × 2.6 = 454 mm^2	7.6 × 8.5 = 51 mm^2
Modified criterion (present work)	167.4 × 3.1 = 519 mm^2	5.1 × 5.8 = 23 mm^2

Table 8. Modified Niyama's criteria outcomes: comparison among different casting speeds.

	Standard casting speed	High casting speed
Central part (A)	160.6 × 2.1 = 337 mm^2	167.4 × 3.1 = 538 mm^2
Triple point (B)	6.1 × 5.8 = 28 mm^2	5.1 × 5.8 = 23 mm^2

region accounts for 27% of transversal section; it shall be pointed out that in this case M-EMS is acting.

For internal quality assessment, following conclusions might be done. There is porosity, anyhow its extension is limited compared to the transversal section, also at high casting speed; equiaxed area develops in the inner part of beam blank and decreases if casting speed increases. These outcomes are expected and confirm what has been learnt for convex cast shapes.

It shall be pointed out that beam blanks, due to their shape, can be prone to "web opening" and bulging in case of insufficient supporting structure during secondary cooling; the higher the casting speed, the longer shall be the containment and support length. These are mechanical phenomena that are not included in the presented model.

8. Conclusions

A 2D thermal transient travelling slice model has been used to predict the porosity occurrence and the microstructure (by means of well-known Niyama's and Hunt's criteria) of a continuously cast steel section, focusing on complex shapes (*i.e.* having convex and concave parts). Model has been improved considering the thermal effect of EMS devices also. To validate the proposed model, the case of a billet and of a bloom were firstly considered. The predicted cast structures were compared with real macroetches taken from steel production

plants, showing the capability of the proposed procedure to catch both porosity and columnar to equiaxed transition (CET). A deepening on both criteria has been made, making a fine tuning on the governing parameters on bloom case: this has led to a new exponent q for modified Niyama's criterion, widening its applicability to products characterized by an aspect ratio that differs from the unit; the reason of the shape dependance expressed by means of an increase of q exponent has been recognized to be related to the influence of SDAS. The outcomes show a good agreement between calculated and measured parameters. Only quite slight disagreement are observed, that can be ascribed to the non-symmetric real thermal boundary condition, which are not included in the billet and bloom models due to intrinsic hypothesis of double symmetry contained in the travelling slice approach; moreover, it has been verified how the thermal history (*i.e.* low or high secondary cooling practices) may affect the porosity. It shall be noted that location of porosity areas, as well as their extension, can be correctly detected only with a careful choice of the q exponent of the Niyama's parameter (q=0.895 for billet, q=1.3 for bloom). It is thus made available a quick tool for sensitivity studies on the main process variables such as steel grades, casting speed, secondary cooling intensity and use of EMS devices.

Finally, the model has been applied to investigate the feasibility of a possible future set-up for a high-speed beam blank: modified Niyama's (as proposed in this work) and Hunt's criteria has been chosen instead of original ones due to the higher precision shown for the bloom case.

In the case of standard casting speed, as expected, porosity is present, anyhow its extension is limited compared to the transversal section and thus certainly acceptable. At high casting speed a significant increase of porosity is observed (+ 60%), nevertheless still largely fulfilling the quality requirements for these cast products. Equiaxed area develops in the inner part of beam blank and decreases if casting speed increases.

It has to be noted that also other factors, such as bulging (*i.e.* the deformation induced by liquid steel pressure), may become a limiting factor for the productivity increase. The whole assessment on this cutting-edge process technology will continue, trying to estimate other eventual limiting factors arising from other fields, if any.

Statement for Conflict of Interest

G. B. declares to be an employee of Danieli & C. Officine Meccaniche SpA headquartered in Buttrio (Italy). F. D. B. declares no conflict of interest.

Acknowledgments

The authors would like to thank professor Hee-Soo Kim of Chosun University (Korea) for the fruitful opinion exchange.

REFERENCES

1) J. Madias, C. Genzano, M. Oropeza and C. Moss: *Iron & Steel Technology*, August (2018), 130.
2) B. G. Thomas: S*teel Research Int*, (2017), 1. https://doi.org/10.1002/srin.201700312
3) J. D. Hunt: *Material Science and Engineering*, **65** (1984), 75.
4) E. Niyama, T. Uchida, M. Morikawa and S. Saito: *International cast metals journal*, **7** (1982), 52.
5) R. Tavakoli: *Int. journal of Advanced Manuf. Technology*, (2014), 569. https://doi.org/10.1007/s00170-014-5995-0
6) A. S. Jabur and F. M. Kushnaw: *Journal of Appl. & Computat. Mathematics*, **6** (2017), 1. https://doi.org/10.4172/2168-9679.1000371
7) K. Mramor, V. Hatic and B. Šarler: Proceedings of International Conference on Computational & Experimental Engineering and Science, Tokyo, (2019), 1, CD-ROM.
8) C. Zhang, Y. Bao, M. Wang and L. Zhang: *Archives of foundry engineering*, **16** (2016), 27.
9) Z. Yu, H. Zhang, X. Wang and X. Wu: *La Metallurgia Italiana*, **16** (2020), 37.
10) K. D. Carlson and C. Beckermann: *Metallurgical and materials transaction A*, **40A** (2009), 163. https://doi.org/10.1007/s11661-008-9715-y
11) M. Kang, H. Gao, J. Wang, L. Ling and B. Sun: *Materials*, **6** (2013), 1789. https://doi.org/10.3390/ma6051789
12) H. Shibata, S. Itoyama, Y. Kishimoto, S. Takeuchi and H. Sekiguchi: *ISIJ Int.*, **46** (2006), 921. https://doi.org/10.2355/isijinternational.46.921
13) G. Straffelini, L. Lutterotti, M. Tonolli and M. Lestani: *ISIJ Int.*, **51** (2011), 1448. https://doi.org/10.2355/isijinternational.51.1448
14) S. K. Choudhary and S. Ganguly: *ISIJ Int.*, **47** (2007), 1759. https://doi.org/10.2355/isijinternational.47.1759
15) Q. Dong, J. Zhang and X. Zhao: *Met. Res. & Technology*, **114** (2017), 303. https://doi.org/10.1051/metal/2017004
16) M. Vynnycky: *Journal of Mathematics in Industry*, **10:14** (2020), 1. https://doi.org/10.1186/s13362-020-00084-2
17) H. S. Kim, J. J. Kim and K. S. Oh: *Journal of Materials Engineering and Performance*, (2022), 4064. https://doi.org/10.1007/s11665-023-07947-w
18) H. S. Kim and J. J. Kim: *Korean Journal of Metals and Materials*, **61(1)** (2023), 60.
19) M. El-Bealy and B. G. Thomas: *Metallurgical and materials transaction B*, **27B** (1996), 689.
20) IDS – Solidification package for steels – version 2.0, Casim Consulting Oy, (2016).
21) S. Kunstreich: *La Revue de Métallurgie*, **100(4)** (2003), 395.
22) S. Kunstreich: *La Revue de Métallurgie*, **100(11)** (2003), 1043.
23) K. Ayata, T. Inoue, H. Mori, S. Ishiguro, H. Nakata, T. Murakami and T. Kominami: *La Revue de Métallurgie*, **98(11)** (2001), 1025.
24) X. Geng, X. Li, F. B. Liu, H. B. Li and Z. H. Jiang: *Ironmaking and Steelmaking*, **42(9)** (2015), 675. https://doi.org/10.2355/isijinternational.46.903
25) M. Yamazaki, Y. Natsume, H. Harada and K. Ohsasa: *ISIJ Int*., **46** (2006), 903. https://doi.org/10.2355/isijinternational.46.903
26) P. Lan, L. Li, S. Wang and J. Zhang: *Steel Research International*, **96** (2025), 1. https://doi.org/10.1002/srin202400595
27) H. An, Y. Bao, M. Wang and L. Zhao: *Met. Res. Technology*, **115** (2018), 1. https://doi.org/10.1051/metal/2017075
28) A. Maurya and P. K. Jha: *Applied Mathematical Modelling*, (2017), 736. https://doi.org/10.1016/j.apm.2017.02.029
29) G. Bazzaro and F. De Bona: *Metals*, **13** (2023), 1505. https://doi.org/10.3390/met13091505
30) K. J. Schwerdtfeger: The making shaping and treating of steel – Casting volume, The AISE steel foundation, Pittsburg, (2003), Chapter 4, 1.
31) S. Louhenkilpi, J. Miettinen and L. Holappa: *ISIJ Int.*, **46** (2006), 914. https://doi.org/10.2355/isijinternational.46.914
32) H. Taheri, E. Hajidavalloo and M. Reza Saffarian: *Journal of the Minerals, Metals and Materials Society*, **77** (2025), 6010. https://doi.org/10.1007/s11837-025-07173-w
33) D. Fátima Gomes, B. Martins Braga, R. Parreiras Tavares and M. Covcevich Bagatini: *Computer Methods in Materials Science*, **21(3)** (2021), 149. https://doi.org/10.7494/cmms.2021.3.0735